Communication

Compact Ultrawideband Antenna on Folded Ground Plane

Seongjung Kim and Sangwook Nam

***Abstract*— A compact ultrawideband antenna on folded ground plane is proposed, which is a compact and low-profile structure. The proposed antenna mimics the operation of a unit element of the tightly coupled dipole array (TCDA) with modified boundary condition. The antenna does not have the PMC boundary required by the original TCDA, which makes the implementation and the impedance matching of the proposed antenna easy. All the design procedures are explained and confirmed by the EM simulation. The measured results show that the impedance bandwidth (IBW) is 0.72–3.43 GHz (130.6%) for the VSWR < 2 and that the radiation efficiency is over 89% in the operating band. The average peak gain is 2.33 dBi. These results are in good agreement with those of the simulation. The proposed antenna is compact, with an electrical size ($\kappa\alpha$) of 0.82 at the lowest operating frequency and an overall dimension of $0.17\lambda_{low} \times 0.17\lambda_{low} \times 0.11\lambda_{low}$ in terms of the wavelength at the lowest operating wavelength.**

***Index Terms*— Compact antenna, high radiation efficiency, low-profile antenna, tightly coupled dipole array (TCDA), ultrawideband (UWB) antenna.**

TABLE I

IN COMPARISON WITH COMPACT AND WIDEBAND ANTENNAS

Ref.	Type	Radiation Pattern	Antenna Size (unit: λ_{low}^3, $\kappa\alpha$)	Gain (unit: dBi)	IBW (unit: GHz, %)
[14]	2D	Bi-	0.22 × 0.22 × 0.009, 0.96	1.2–4.2	2.6–11.12, 124.2
[15]	2D	Bi-	0.25 × 0.12 × 0.008, 0.87	1.0–4.0	3.1–11.0, 112.1
[16]	3D	Bi-	0.2 × 0.2 × 0.06, 0.91	1.9–3.9	0.3–0.46, 43.0
[17]	3D	Uni-	0.24 × 0.1 × 0.05, 1.17	2.0–3.2	1.03–1.85, 57
This Work	3D	Uni-	0.17 × 0.17 × 0.11, 0.82	0.55–3.74	0.72–3.43, 130.6

I. INTRODUCTION

Ultrawideband (UWB) antennas are widely used in many communication applications such as high-data rate communication, high-resolution radar systems, and wireless image sensing [1]. However, the designers of the UWB antenna face many requirements, such as compact size, high radiation efficiency, low profile, and high directivity, which are in tradeoff relation. Consequently, there have been many trials to improve the overall performances of the UWB antennas with respect to small size, wideband, and high radiation efficiency. For instance, several variations of the Vivaldi antenna, the Yagi–Uda antenna, the log-periodic antenna, and the cavity-backed antenna have been proposed to make the wideband and high-directive antenna in [2]–[11]. However, the resulting size is inevitably large. Also, the wideband micro-strip antennas are popular for their compactness and low-profile [12], [13]. Recently, very compact, UWB, and stable radiation pattern antennas have been proposed [14]–[17].

There is an interesting extremely wideband array antenna structure with a low profile, the so-called tightly coupled dipole array (TCDA) antenna [18]. This TCDA antenna is very attractive due to its low profile and has a stable radiation pattern over the UWB by using the coupling capacitance between the adjacent dipoles as a compensating element of the inductance of the ground plane [19]–[23]. The operating principle will be explained briefly in the following section. However, the TCDA antennas were designed only for two-dimensional array (2-D TCDA), before the one-dimensional TCDA (1-D TCDA) dual polarized antenna was proposed in [24]. The 1-D TCDA operates like the original TCDA by using a conducting strip wall with a thin ferrite layer to approximate the PEC/PMC boundary condition of the TCDA unit cell for vertical/horizontal polarization. By these walls, image dipoles are formed on both side of 1-D TCDA such as 2-D array.

In this communication, a single polarized ultrawide impedance bandwidth (IBW) antenna is proposed with a relatively regular beam pattern compared with previous UWB antennas. The proposed antenna is inspired by communication [24] but without PMC walls. In the proposed structure, the PEC and the PMC boundaries required by original TCDA are implemented by conducting walls with a finite height and open space, respectively. This modification of the PMC boundary has several advantages. First, it does not require PMC walls, which simplifies the implementation of the antenna and increases the radiation efficiency by avoiding the lossy ferrite layer. Second, the self-resonance occurring in the unit cell structure of the 2-D TCDA, when the distance between the PMC walls is one wavelength, can be avoided so that the impedance matching in the high-frequency band is possible. Third, the directivity of the proposed antenna is stable with different frequencies.

The communication is organized as follows. In Section II, the theory of the TCDA is reviewed briefly and the boundary conditions to be used in the proposed antenna scenario are compared. From this comparison, the procedure to derive the proposed antenna structure is explained step by step. In Section III, measured results for the proposed single antenna are shown, and a performance comparison is presented in Table I. In Section IV, conclusions about the findings are drawn.

II. ANTENNA DESIGN AND ANALYSIS

A. Brief Introduction to the 2-D TCDA

In this section, the 2-D TCDA is briefly introduced. The basic TCDA structure is shown in Fig. 1(a) and its boundary condition for a unit element is shown in Fig. 1(b), which consists of the PEC on both ends of the dipole and the PMC on both sides. This PEC/PMC virtual

Manuscript received October 31, 2018; revised December 22, 2019; accepted February 18, 2020. Date of publication March 9, 2020; date of current version October 6, 2020. This work was supported by the Global Frontier Program through the National Research Foundation of Korea (NRF) funded by the Ministry of Science, ICT and Future Planning under Grant NRF-2014M3A6B3063708. *(Corresponding author: Seongjung Kim.)*

The authors are with the School of Electrical and Computer Engineering, Institute of New Media Communication (INMC), Seoul National University, Seoul 08826, South Korea (e-mail: sjkim@ael.snu.ac.kr).

Color versions of one or more of the figures in this communication are available online at http://ieeexplore.ieee.org.

Digital Object Identifier 10.1109/TAP.2020.2977818

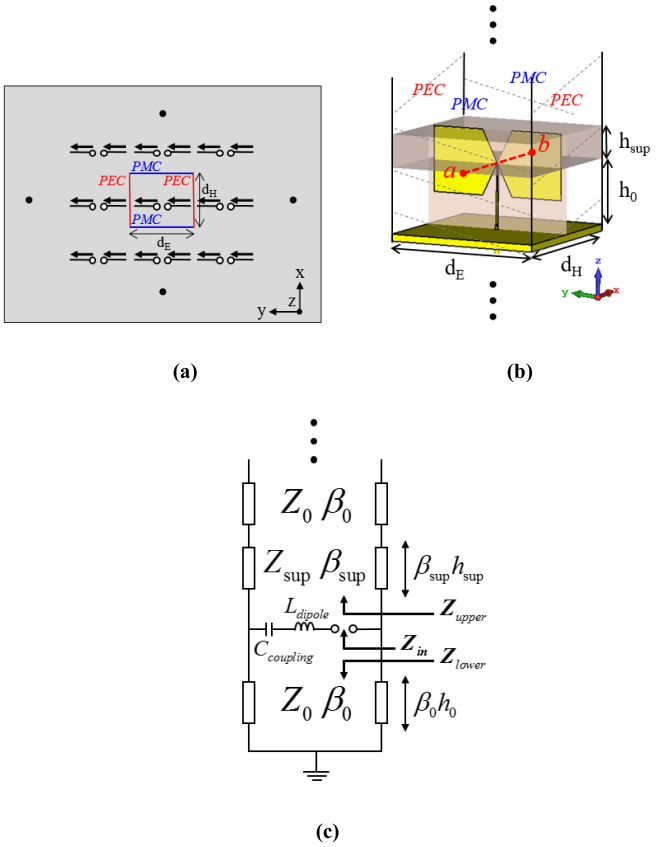

Fig. 1. (a) Conventional 2-D TCDA structure (top view). (b) Unit cell structure with the proper boundary condition. (c) Equivalent circuit of a unit cell. h_{sup} and h_0 represent the thickness of the superstrate and the space between the superstrate and the ground, respectively.

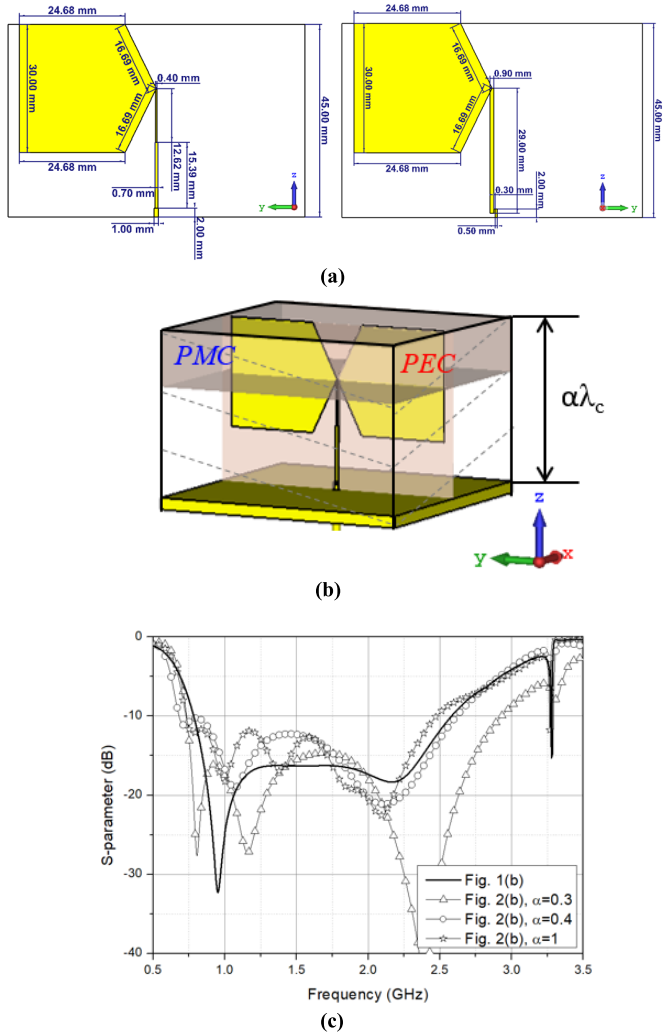

Fig. 2. Structure and the impedance characteristic (simulation) of a unit cell antenna with different heights of the PEC/PMC wall. (a) Front (left) and back (right) side of the dipole PCB. (b) Configuration of the antenna with a finite height of the PEC/PMC wall where λ_c is 150 mm. (c) Comparison of the impedance matching property corresponding to the infinite and finite heights of the PEC/PMC boundary.

waveguide has a Z_0 characteristic impedance, which is determined by lengths d_E and d_H, and a β_0 propagation constant in the free space. Z_{sup} and β_{sup} represent a characteristic impedance and a propagation constant in the superstrate, respectively. The equivalent circuit of the unit cell is shown in Fig. 1(c) [18].

At a low-frequency band, Z_{lower} is inductive. The basic principle of the TCDA to reduce the antenna height is to cancel the inductive Z_{lower} by $C_{coupling}$, which is a gap capacitance between the tightly coupled dipoles. On the other hand, at a high-frequency band, which means that the length of the shorted transmission line is longer than the quarter wavelength, Z_{lower} looks like a capacitor. Then, the capacitive Z_{lower} is canceled by L_{dipole}, which is self-inductance of the dipole. In addition, the superstrate is helpful for a wideband impedance matching and directive radiation pattern. Finally, the antenna input impedance Z_{in} with an operating angular frequency ω, given in (1), can be relatively constant from a low- to high-frequency band. As a result, the TCDA antenna can have a UWB characteristic with a low profile

$$Z_{in} = j\omega L_{dipole} + \frac{1}{j\omega C_{coupling}} + Z_{lower} \parallel Z_{upper}. \quad (1)$$

B. Configuration of the Proposed Antenna

The height of the PEC/PMC boundary should be reduced to a finite value in order to be implemented in a single antenna, as shown in Fig. 2(b), that has a PCB whose dimension is shown in Fig. 2(a). Fig. 2(c) shows the impedance matching characteristic of the unit cell element antenna derived from the 2-D TCDA with various heights of the PEC/PMC boundary. It is noticed that the higher the boundary wall is, the closer the impedance characteristic is to the ideal unit cell impedance characteristic corresponding to Fig. 1(b). However, a higher boundary means that the advantage of a low profile, which is the greatest advantage of the TCDA, is lost. Hence, it is necessary to find a height that is as small as possible at which the impedance matching characteristic is similar to the ideal unit cell antenna. We find that the height can be reduced to a wavelength of 0.3 (45 mm) by using the EM simulation. Furthermore, even if the height is reduced, it shows a better impedance matching characteristic, especially for a high-frequency band. Thus, in this communication, the height of 0.3 wavelength was selected for the boundary wall.

The configuration of the proposed unit cell antenna is shown in Fig. 3(a), which is fed by single-ended coaxial cable and the same PCB, as shown in Fig. 2(a), is used. The dipole antenna is designed on the Taconic TLY-5 PCB ($\varepsilon_r = 2.2$, $\tan\delta = 0.0009$), with a thickness of 0.25 mm and the superstrate that is composed of a stack of TLY-5 boards with a thickness of 15 mm. The PEC walls are located on both ends to reproduce the PEC boundary condition of the unit cell of a conventional TCDA antenna.

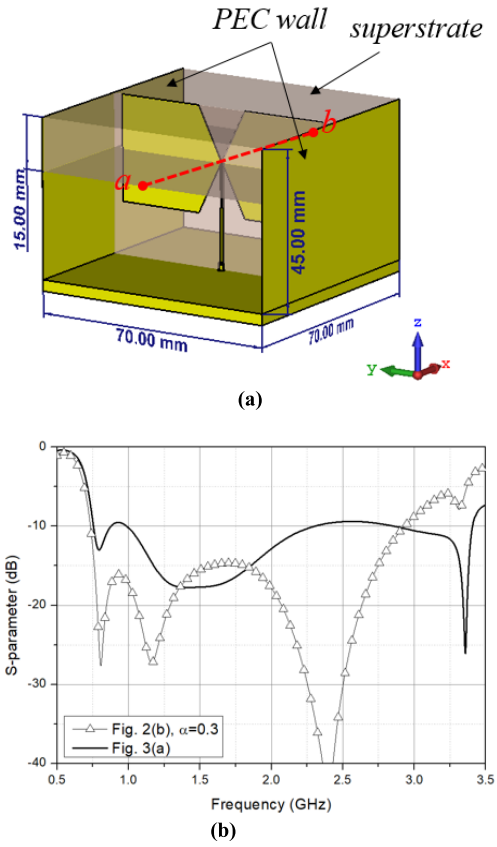

Fig. 3. (a) Structure of the proposed PEC/OPEN boundary antenna. (b) Comparison of the antennas using the proposed PEC/OPEN boundary and a finite height of the PEC/PMC boundary.

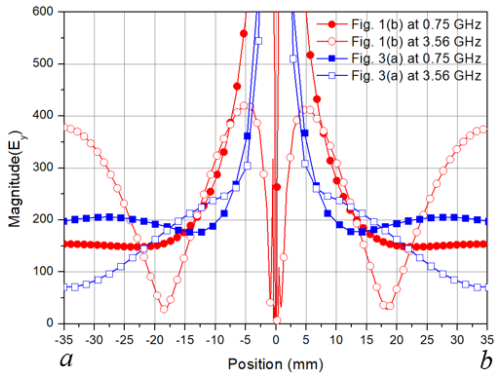

Fig. 4. Y-component electric field intensity of Figs. 1(b) and 3(a) on the dashed line $(a - b)$.

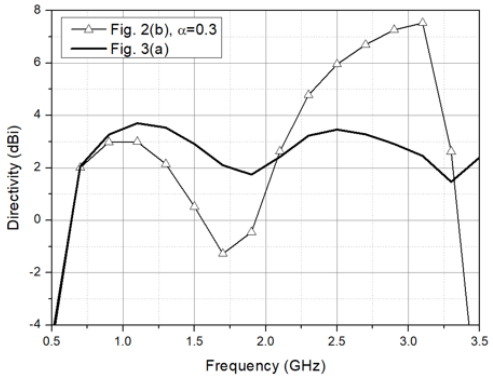

Fig. 5. Directivity to broadside direction of Figs. 2(b) and 3(a).

In general, it is difficult to implement PMC walls. In addition, they can cause magnetic losses and degrade the radiation efficiency. Therefore, in this communication, the PMC walls on both sides are replaced by an open space boundary.

Fortunately, as shown in Fig. 3(b), the impedance matching of the proposed antenna is also good in the low- and mid-frequency band and even better around 3.3 GHz, in comparison with the impedance matching with PMC walls. Although the antenna shown in Fig. 1(b) with an infinite side wall is a single antenna, the antenna input impedance is the same with a 2-D array due to image dipoles [24]. It follows, therefore, that the impedance matching of the antenna in Fig. 1(b) is poor when the element size is one wavelength [18]. In the following section, the reason for this will be interpreted in terms of electric field distributions. It is worth mentioning that although the equivalent transmission line model [Fig. 1(c)] does not represent the proposed antenna exactly due to the finite height of PEC walls and the absence of PMC walls, it may explain the principle behind the wideband characteristics of the proposed antenna to some degree.

C. Electric Field Distribution Analysis

Fig. 4 shows y-component electric field intensity in the proposed open boundary [Fig. 3(a)] and an infinite height PEC/PMC boundary [Fig. 1(b)] on the red-dashed line $(a - b)$ denoted in Figs. 1(b) and 3(a), respectively.

At 0.75 GHz, the wavelength is very long in comparison with the unit cell size, so there is little change in the field profile with space in Fig. 4. As a result, it is almost similar to the PMC boundary, even though the side is an open boundary and can have an impedance matching characteristic of the PEC/PMC boundary at a low-frequency band.

On the other hand, at 3.56 GHz, the fields of the proposed open boundary antenna and the PEC/PMC boundary antenna are completely different. The difference comes from the fact that there is a strong resonance in the PEC/PMC boundary antenna at 3.56 GHz, when the distance between the PMC walls is approximately one wavelength at 3.56 GHz, whereas a traveling wave exists along the side for the open boundary case. This can be understood by the fact that there are nodes of y-component electric field intensity for the standing wave around $x = \pm 20$ mm, while there is no node for the traveling wave. As a result, the antenna impedance of the PEC/PMC boundary antenna becomes very large at this frequency. On the other hand, if the PMC walls are removed, there is no self-resonance or a standing wave. Therefore, only the traveling wave can be observed. This open boundary can be advantageous for a broadband characteristic, especially for a high-frequency band. Although the radiation power in the main radiation lobe of the proposed antenna is wasted by removing the PMC walls in the high-frequency band, it helps in matching the impedance and makes the directivity of the proposed antenna [Fig. 3(a)] more stable than that of the antenna over the wideband [Fig. 2(b)], as shown in Fig. 5.

III. Simulated and Experimental Results for the Proposed Single Antenna

The EM simulation of the proposed antenna is performed by the CST commercial EM tool and the prototype of the antenna is shown in Fig. 6. The superstrate is supported by the PEC walls

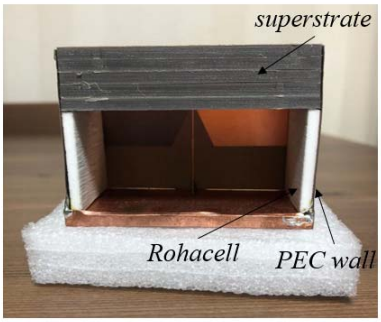

Fig. 6. Prototype of the proposed antenna.

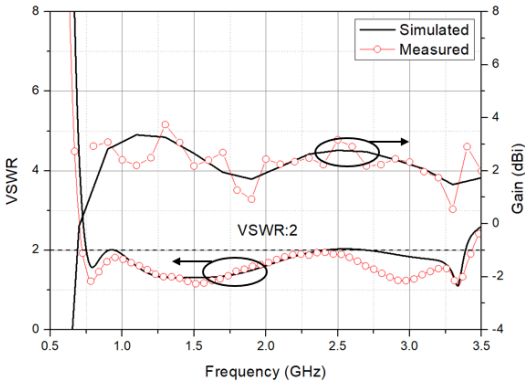

Fig. 7. VSWR and the peak gain of the proposed antenna.

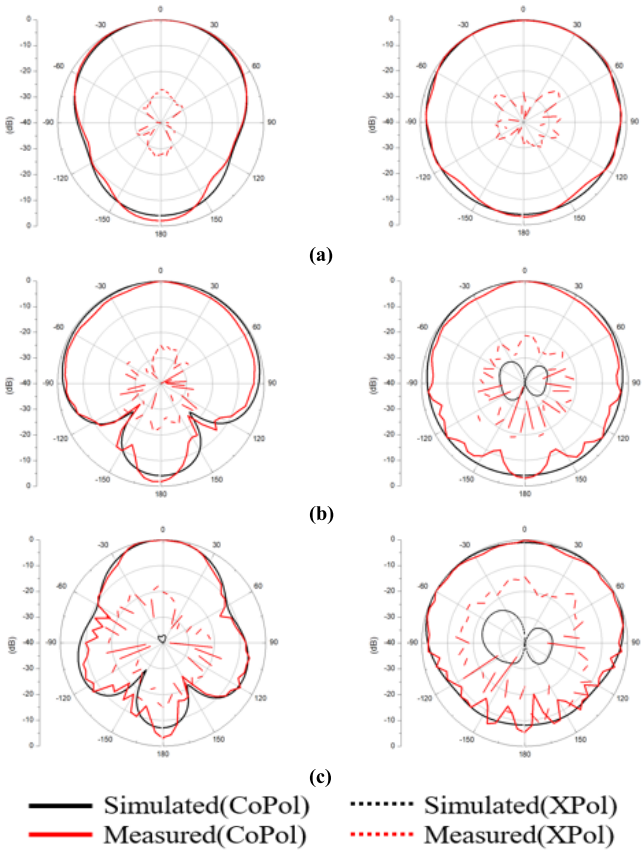

Fig. 8. Normalized gain pattern of the proposed antenna on the E-plane (left) and the H-plane (right) at (a) 1 GHz, (b) 2 GHz, and (c) 3 GHz.

and some Rohacell materials, whose relative permittivity is nearly one. In Fig. 7, the VSWR and the peak gain of the antenna show a good agreement between the simulation results and the

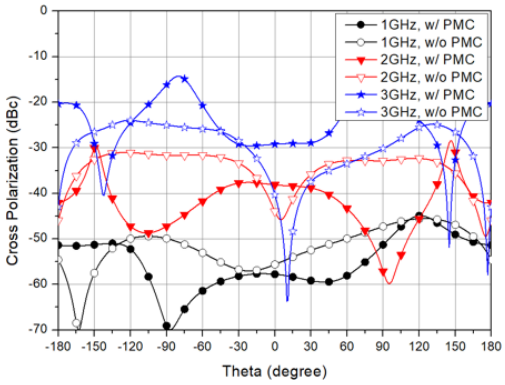

Fig. 9. Simulated cross-polarization pattern of Fig. 2(b) ($\alpha = 0.3$) with and without PMC walls.

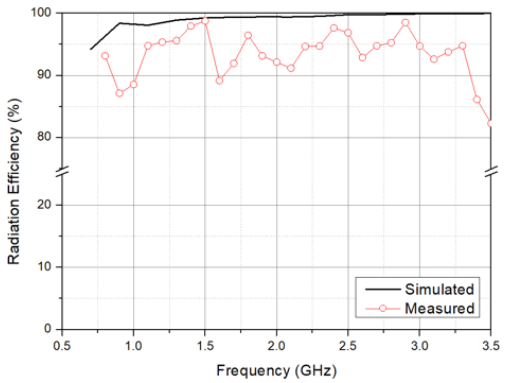

Fig. 10. Radiation efficiency of the proposed antenna.

measurement results. The IBW for the VSWR <2 has the simulation result of 0.75–3.39 GHz (127.5%) and the measurement result of 0.72–3.43 GHz (130.6%). The height is $0.11\lambda_{\text{low}}$ in terms of the lowest operating wavelength. The average value of the peak gain has a simulation result of 2.46 dBi and a measurement result of 2.33 dBi within the IBW. Fig. 8 shows the normalized gain pattern of the copolarization of the antenna at 1, 2, and 3 GHz. The measured cross-polarization in the broadside direction is less than -15 dBc within the operating band. The gain patterns are relatively directive on the E-plane and the back-lobe level is less than -4 dB within the operating band. Fig. 9 shows the simulated cross-polarization pattern of Fig. 2(b) with $\alpha = 0.3$. Except at 1 GHz, the cross-polarization level in the broadside direction without PMC walls is lower than with PMC walls.

Table I shows the comparison with the wideband, compact, stable radiation pattern antennas. Note that "κ" is the wave number with the lowest operating frequency in the free space and "α" is the radius of the sphere, including the antenna. The radiation patterns of the antennas in [14] and [15] are bidirectional to the broadside and backside. The radiation pattern of the antenna in [16] is side and that in [17] is directional to the broadside. Although the volume of the proposed antenna is larger than that of the others, it has the smallest κa and a unidirectional pattern. Even though $\kappa\alpha$ of the proposed antenna is 0.82 and the IBW is 130.6%, which can be said is a compact and UWB antenna, the radiation efficiency is 89% or more in the IBW, as shown in Fig. 10. Among the compared antennas, this work antenna is smaller than the others because the TCDA can have a low-frequency band.

IV. Conclusion

In this communication, a compact UWB and broadside radiated antenna is proposed; it uses the folded ground plane. The radiation pattern is directional in the E-plane and omnidirectional in

the H-plane. Its UWB and low-height characteristics are inherited from the original TCDA characteristics. The PMC boundary condition required by the TCDA is replaced by an open space, which makes the implementation of the antenna easy. This also helps avoid the self-resonance of the ideal TCDA structure so that the IBW of the antenna becomes even wider. The measurement results of the proposed antenna are in good agreement with the simulation results. Finally, this antenna is expected to be used in many applications of the UWB array antennas.

REFERENCES

[1] G. Adamiuk, T. Zwick, and W. Wiesbeck, "UWB antennas for communication systems," *Proc. IEEE*, vol. 100, no. 7, pp. 2308–2321, Jul. 2012.

[2] Y. Xu, J. Wang, L. Ge, X. Wang, and W. Wu, "Design of a notched-band vivaldi antenna with high selectivity," *IEEE Antennas Wireless Propag. Lett.*, vol. 17, no. 1, pp. 62–65, Jan. 2018.

[3] I. T. Nassar and T. M. Weller, "A novel method for improving antipodal vivaldi antenna performance," *IEEE Trans. Antennas Propag.*, vol. 63, no. 7, pp. 3321–3324, Jul. 2015.

[4] J. Bang, J. Lee, and J. Choi, "Design of a wideband antipodal vivaldi antenna with an asymmetric parasitic patch," *J. Electromagn. Eng. Sci.*, vol. 18, no. 1, pp. 29–34, Jan. 2018.

[5] Z. Yang, L. Zhang, and T. Yang, "A microstrip magnetic dipole Yagi–Uda antenna employing vertical i-shaped resonators as parasitic elements," *IEEE Trans. Antennas Propag.*, vol. 66, no. 8, pp. 3910–3917, Aug. 2018.

[6] X. Wei, J. Liu, and Y. Long, "Printed log-periodic monopole array antenna with a simple feeding structure," *IEEE Antennas Wireless Propag. Lett.*, vol. 17, no. 1, pp. 58–61, Jan. 2018.

[7] L. Ge and K. M. Luk, "A magneto-electric dipole for unidirectional UWB communications," *IEEE Trans. Antennas Propag.*, vol. 61, no. 11, pp. 5762–5765, Nov. 2013.

[8] J.-Y. Li, R. Xu, X. Zhang, S.-G. Zhou, and G.-W. Yang, "A wideband high-gain cavity-backed low-profile dipole antenna," *IEEE Trans. Antennas Propag.*, vol. 64, no. 12, pp. 5465–5469, Dec. 2016.

[9] A. Elsherbini and K. Sarabandi, "UWB high-isolation directive coupled-sectorial-loops antenna pair," *IEEE Antennas Wireless Propag. Lett.*, vol. 10, pp. 215–218, 2011.

[10] M. Li and K.-M. Luk, "A differential-fed UWB antenna element with unidirectional radiation," *IEEE Trans. Antennas Propag.*, vol. 64, no. 8, pp. 3651–3656, Aug. 2016.

[11] R. A. Moody and S. K. Sharma, "Ultrawide bandwidth (UWB) planar monopole antenna backed by novel pyramidal-shaped cavity providing directional radiation patterns," *IEEE Antennas Wireless Propag. Lett.*, vol. 10, pp. 1469–1472, 2011.

[12] J. Liang, C. C. Chiau, X. Chen, and C. G. Parini, "Study of a printed circular disc monopole antenna for UWB systems," *IEEE Trans. Antennas Propag.*, vol. 53, no. 11, pp. 3500–3504, Nov. 2005.

[13] J.-H. Kim and B.-G. Kim, "Effect of feed substrate thickness on the bandwidth and radiation characteristics of an aperture-coupled microstrip antenna with a high permittivity feed substrate," *J. Electromagn. Eng. Sci.*, vol. 18, no. 2, pp. 101–107, Apr. 2018.

[14] J. Pourahmadazar, C. Ghobadi, and J. Nourinia, "Novel modified pythagorean tree fractal monopole antennas for UWB applications," *IEEE Antennas Wireless Propag. Lett.*, vol. 10, pp. 484–487, 2011.

[15] H. Yang, X. Xi, Y. Zhao, L. Wang, and X. Shi, "Design of compact ultrawideband slot antenna with improved band-edge selectivity," *IEEE Antennas Wireless Propag. Lett.*, vol. 17, no. 6, pp. 946–950, Jun. 2018.

[16] J. Oh and K. Sarabandi, "Low profile vertically polarized omnidirectional wideband antenna with capacitively coupled parasitic elements," *IEEE Trans. Antennas Propag.*, vol. 62, no. 2, pp. 977–982, Feb. 2014.

[17] A. T. Mobashsher and A. Abbosh, "Slot-loaded folded dipole antenna with wideband and unidirectional performance for L-band applications," *IEEE Antennas Wireless Propag. Lett.*, vol. 13, pp. 798–801, 2014.

[18] B. A. Munk, *Finite antenna arrays and FSS*. Hoboken, NJ, USA: Wiley, 2003.

[19] S. S. Holland and M. N. Vouvakis, "The planar ultrawideband modular antenna (PUMA) array," *IEEE Trans. Antennas Propag.*, vol. 60, no. 1, pp. 130–140, Jan. 2012.

[20] J. P. Doane, K. Sertel, and J. L. Volakis, "A wideband, wide scanning tightly coupled dipole array with integrated balun (TCDA-IB)," *IEEE Trans. Antennas Propag.*, vol. 61, no. 9, pp. 4538–4548, Sep. 2013.

[21] W. F. Moulder, K. Sertel, and J. L. Volakis, "Superstrate-enhanced ultrawideband tightly coupled array with resistive FSS," *IEEE Trans. Antennas Propag.*, vol. 60, no. 9, pp. 4166–4172, Sep. 2012.

[22] I. Tzanidis, K. Sertel, and J. L. Volakis, "UWB low-profile tightly coupled dipole array with integrated balun and edge terminations," *IEEE Trans. Antennas Propag.*, vol. 61, no. 6, pp. 3017–3025, Jun. 2013.

[23] E. Yetisir, N. Ghalichechian, and J. L. Volakis, "Ultrawideband array with 70° scanning using FSS superstrate," *IEEE Trans. Antennas Propag.*, vol. 64, no. 10, pp. 4256–4265, Oct. 2016.

[24] H. Lee and S. Nam, "A dual-polarized 1-D tightly coupled dipole array antenna," *IEEE Trans. Antennas Propag.*, vol. 65, no. 9, pp. 4511–4518, Sep. 2017.